Structure-activity relationships for osmium(II) arene phenylazopyridine anticancer complexes functionalised with alkoxy and glycolic substituents

Needham, R. J., Bridgewater, H. E., Romero-Canelón, I., Habtemariam, A., Clarkson, G. J. & Sadler, P. J.

DOI 10.1016/j.jinorgbio.2020.111154
ISSN 0162-0134

Publisher: Elsevier

Journal of Inorganic Biochemistry 210 (2020) 111154

Contents lists available at ScienceDirect

Journal of Inorganic Biochemistry

journal homepage: www.elsevier.com/locate/jinorgbio

Structure-activity relationships for osmium(II) arene phenylazopyridine anticancer complexes functionalised with alkoxy and glycolic substituents

Russell J. Needham, Hannah E. Bridgewater, Isolda Romero-Canelón, Abraha Habtemariam, Guy J. Clarkson, Peter J. Sadler*

Department of Chemistry, University of Warwick, Gibbet Hill Road, Coventry CV4 7AL, UK

ARTICLE INFO

Keywords:
Organometallic complexes
Half sandwich arene complexes
Osmium complexes
Anticancer
Aqueous solubility and stability
Mechanism of action

ABSTRACT

Twenty-four novel organometallic osmium(II) phenylazopyridine (AZPY) complexes have been synthesised and characterised; [Os(η^6-arene)(5-RO-AZPY)X]Y, where arene = *p*-cym or bip, AZPY is functionalized with an alkoxyl (O-R, R = Me, Et, ^{n}Pr, ^{i}Pr, ^{n}Bu) or glycolic (O-{CH_2CH_2O}$_n$R*, n = 1–4, R* = H, Me, or Et) substituent on the pyridyl ring *para* to the azo-bond, X is a monodentate halido ligand (Cl, Br or I), and Y is a counter-anion (PF_6^-, $CF_3SO_3^-$ or IO_3^-). X-ray crystal structures of two complexes confirmed their 'half-sandwich' structures. Aqueous solubility depended on X, the AZPY substituents, arene, and Y. Iodido complexes are highly stable in water (X = I ⋙ Br > Cl), and exhibit the highest antiproliferative activity against A2780 (ovarian), MCF-7 (breast), SUNE1 (nasopharyngeal), and OE19 (oesophageal) cancer cells, some attaining nanomolar potency and good cancer-cell selectivity. Their activity and distinctive mechanism of action is discussed in relation to hydrophobicity (RP-HPLC capacity factor and Log $P_{o/w}$), cellular accumulation, electrochemical reduction (activation of azo bond), cell cycle analysis, apoptosis and induction of reactive oxygen species (ROS). Two complexes show ca. 4× higher activity than cisplatin in the National Cancer Institute (NCI) 60-cell line five-dose screen. The COMPARE algorithm of their datasets reveals a strong correlation with one another, as well as anticancer agents olivomycin, phyllanthoside, bouvardin and gamitrinib, but only a weak correlation with cisplatin, indicative of a different mechanism of action.

1. Introduction

Some of the first phenylazopyridine (AZPY) complexes of Ru(II) reported in 1979 exhibited strong dπ-pπ metal-ligand interactions, which endow them with high stability [1]. These effects were later utilised in both Ru(II) and Os(II) AZPY arene anti-cancer complexes [2–6]. Interestingly, Os(II) arene complexes of azobipyridine and Ru(II) arene complexes of AZPY have ligand-based redox properties [2,7]. Their cyclic voltammogram reduction potentials can be attributed to reduction of the azo-bond, which contains a low lying π*-orbital capable of accepting two electrons. Previously-reported piano-stool Os(II) arene AZPY complexes exhibit potent anti-proliferative activity against a variety of cancer cell lines [8]. Their mechanism of action differs greatly from earlier Os(II) arene complexes with σ-donor bidentate ligands, which rely primarily on dissociation of a monodentate ligand followed by DNA nucleobase binding [9–13]. In contrast, the strong π-acceptor character of AZPYs produces different characteristics, such as resistance towards hydrolysis and a mechanism of action involving increased levels of intracellular reactive oxygen species (ROS) [4–6,14].

Current structure-activity relationships (SARs) reported for Os(II) arene AZPY complexes include the ability of monodentate iodido ligands to improve anti-cancer activity significantly over chlorido ligands, enhancement of activity by biphenyl (bip) over *p*-cymeme (*p*-cym) arene ligands, and ability of AZPY ligand substituents positioned on the pyridyl and phenyl moieties *para* to the azo-bond also to enhance activity [4,5,15]. Anticancer drug design concepts often make use of Lipinski's 'rule of five' (Ro5) to determine whether a drug candidate has pharmacological properties which make it suitable for absorption, distribution, metabolism and excretion within the human body [16,17]. A variation to Ro5 suggests that the effective range of Log $P_{o/w}$ is −0.4 to +5.6 [18] and varying ligand substituents is an effective strategy for tuning metallodrug lipophilicity, cell uptake and activity. The inclusion of alkyl substituents generally increases drug lipophilicity [19] and in a class of Pt(IV) drugs, long chain alkyl substituents that mimic fatty acids improved cell uptake and human serum albumin interactions, resulting in enhanced activity [20]. In contrast, polyethylene glycol is a strongly solubilising substituent, which improves the aqueous solubility of hydrophobic molecules [21,22]. Moreover, polyethylene glycol can

* Corresponding author.
E-mail address: p.j.sadler@warwick.ac.uk (P.J. Sadler).

https://doi.org/10.1016/j.jinorgbio.2020.111154
Received 9 April 2020; Received in revised form 9 June 2020; Accepted 11 June 2020
Available online 24 June 2020

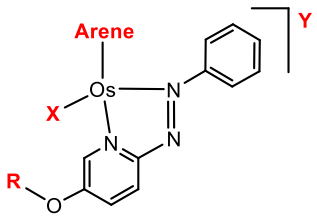

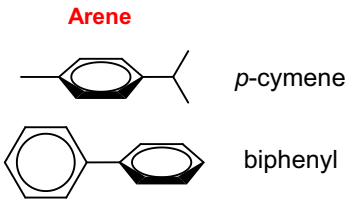

R = Alkyl group

R = 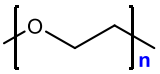

Complex	Arene	X	Y	R	Complex	Arene	X	Y	R*	n
1	*p*-cym	I	PF_6	Me	**13**	*p*-cym	Cl	PF_6	H	1
2	*p*-cym	I	CF_3SO_3	Me	**14**	*p*-cym	Br	PF_6	H	1
3	*p*-cym	Cl	PF_6	Et	**15**	*p*-cym	I	PF_6	H	1
4	*p*-cym	Br	PF_6	Et	**16**	bip	I	PF_6	H	1
5*	*p*-cym	I	PF_6	Et	**17**	*p*-cym	I	PF_6	H	2
6	*p*-cym	I	CF_3SO_3	Et	**18**	*p*-cym	I	PF_6	Me	2
7	*p*-cym	I	IO_3	Et	**19**	*p*-cym	I	PF_6	Et	2
8	bip	I	PF_6	Et	**20**	bip	I	CF_3SO_3	Et	2
9	bip	I	CF_3SO_3	Et	**21**	*p*-cym	I	PF_6	H	3
10	*p*-cym	I	PF_6	^{n}Pr	**22**	*p*-cym	I	PF_6	Me	3
11	*p*-cym	I	PF_6	^{i}Pr	**23**	*p*-cym	I	PF_6	Et	3
12	*p*-cym	I	PF_6	^{n}Bu	**24**	*p*-cym	I	PF_6	H	4

Fig. 1. Osmium(II) arene phenylazopyridine complexes synthesised, characterised and studied in this work.
*Complex previously synthesised and reported [32].

be utilised to encapsulate hydrophobic organic anticancer drugs as nano-micelles, drastically improving their bioavailability and delivery [23]. There appear to be no reports of varying the chain length and tail groups of glycolic substituents to modulate metallodrug properties, however, they have been incorporated into homobinuclear Au(I) and Ru(II) anticancer complexes to create variable length linkages between metal centres [24].

Here we explore the effects of changes in the charge polarisation of Os(II) arene AZPY complexes on activity towards cancer cells, using a variety of alkoxy and glycolic side-chains on AZPY ligands. A series of 24 new Os(II) arene AZPY complexes have been synthesised and the SARs explored for activity against A2780 human ovarian cancer cells, solubility in aqueous media, RP-HPLC capacity factors (lipophilicity), and cellular uptake. We also explore variation of the counter-anion as a means of improving aqueous solubility. Fig. 1 lists the synthesised complexes **1–24**. Selected complexes were further screened against other cancer and normal cell lines (MCF-7 breast, SUNE1 nasopharyngeal, OE19 oesophageal and MRC-5 lung), and their ability to induce apoptosis, elevate ROS levels, and induce cell cycle arrest in A2780 cells were studied.

2. Experimental

2.1. Materials

$OsCl_3{\cdot}3H_2O$ was purchased from either Sigma Aldrich (UK) or Heraeus (South Africa). Most chemicals were purchased from Sigma Aldrich (UK): α-terpinene, biphenyl, 2-amino-5-fluoropyridine, nitrosobenzene, ammonium hexafluorophosphate, ammonium triflate, potassium iodate. The alcohols/glycols used for synthesising RO-AZPY ligands were also purchased from Sigma Aldrich, with the exception of ethylene glycol and diethylene glycol, which were obtained from Alfa Aesar (UK). All other organic solvents and reagents for synthesis and analysis were purchased from commercial suppliers and were used as received. Dimers; $[Os(\eta^6\text{-}p\text{-cym})X_2]_2$, where X = Cl, Br or I, were prepared according to reported procedures [25–27] as was 2-(phenylazo)-5-fluoropyridine [4]. Dulbecco's Modified Eagle Media, Roswell Park Memorial Institute-1640 cell culture medium, penicillin/streptomycin mixture, foetal bovine serum, L-gutamine, phosphate buffered saline solution (PBS), trypsin, and trypsin/ethylenediaminetetraacetic acid were all purchased from PAA Laboratories GmbH. Cell culture media (500 mL) were supplemented with foetal bovine serum (50 mL), penicillin/streptomycin mixture (5 mL) and L-glutamine (2 mM, 5 mL). Cancer cell lines were purchased from the European Collection of Cell Cultures and Public Health England.

2.2. Synthesis of ligands

2-(Phenylazo)-5-fluoropyridine (100.0 mg, 0.50 mmol) was dissolved in ROH (20 mL) and an aqueous KOH solution (5 mol equiv., 0.4 g/mL, 349 μL) was added. The mixture was heated under reflux or at 120 °C (depending on the b.p. of ROH) for 18 h. The product was extracted with CH_2Cl_2 (50 mL) and washed with water (3 × 50 mL). The CH_2Cl_2 extract was dried over $MgSO_4$, filtered, and the solvent was removed under reduced pressure. Some reaction mixtures required vacuum distillation to remove excess ROH. Where necessary, purification was performed by re-crystallisation or SiO_2 column chromatography and the product was dried overnight on a vacuum line. Characterisation and purification methods used for ligands **L1**-**L13** are reported in the SI.

2.3. Synthesis of complexes

$[Os(\eta^6\text{-arene})X_2]_2$ (where X = Cl, Br or I, and arene = *p*-cym or bip)

was dissolved in EtOH (10 mL), and a solution of RO-AZPY (2.1 mol. equiv., **L1**-**L13**) in EtOH (5 mL) was added drop-wise. The mixture was stirred for 18 h at ambient temperature and NH_4PF_6, $NH_4CF_3SO_3$ or KIO_3 (10 mol. equiv.) was added. Complexes were isolated using either method 1 or 2. Method 1 involves re-crystallisation. Some complexes proved difficult to re-crystallise and method 2 was employed. In some cases, further purification via automated reverse-phase chromatography was required. **Method 1:** The ethanolic mixture was concentrated under reduced pressure to ~3 mL and placed in the freezer (−20 °C) overnight. A dark crystalline precipitate formed which was collected via vacuum filtration, washed with ice-cold EtOH (2 × 1 mL), then Et_2O (2 × 5 mL), and dried overnight in a vacuum desiccator. **Method 2:** The ethanolic mixture was concentrated under reduced pressure to ~3 mL and n-hexane was added (~1 mL). The mixture was placed in a freezer (−20 °C) overnight, forming a dark-brown amorphous residue. The solvents were decanted and the residue was washed with Et_2O (3 × 5 mL). The residue was redissolved in CH_2Cl_2 (5 mL), transferred to a pre-weighed vial, and dried overnight on a vacuum line. Reagent quantities, characterisation and isolation methods employed for complexes **1**–**24** are reported in the SI.

2.4. X-ray crystallography

Crystals of **1** were obtained by cooling a methanolic solution of 1–2 mg/mL in a freezer at −20 °C. Crystals of **8** were obtained by slow evaporation of a methanol solution at ambient temperature. Diffraction data were collected on an Oxford Diffraction Gemini four-circle system with a Ruby CCD area detector. All structures were refined by full-matrix least squares against F^2 using SHELXL 97 and were solved by direct methods using SHELXS(TREF) with additional light atoms found by Fourier methods [28]. Hydrogen atoms were added at calculated positions and refined using a riding model. Anisotropic displacement parameters were used for all non-H atoms; H-atoms were given an isotropic displacement parameter equal to 1.2 (or 1.5 for methyl and NH H-atoms) times the equivalent isotropic displacement parameter of the atom to which they are attached. The data were processed by the modelling program Mercury 1.4.1. X-ray crystallographic data for complexes **1** and **8** have been deposited in the Cambridge Crystallographic Data Centre under the accession numbers CCDC1990713 and CCDC1990712, respectively.

2.5. Hydrolysis studies

Solutions of complexes (100 μM) were prepared in phosphate buffer solution (95 mol equiv., pH 7.4, 5% DMSO) with various concentrations of NaCl; 23 mM (intracellular conditions) and 103 mM (extracellular conditions). The samples were incubated at 37 °C for 0, 2, 12 and 24 h and analysed via reverse-phase high-pressure liquid chromatography (RP-HPLC). No precautions were made to protect samples from air or light.

2.6. RP-HPLC capacity factors

Isocratic RP-HPLC analysis of complexes and uracil was carried out (Instrument and column described in the SI). The mobile phase consisted of H_2O:MeCN (1:1, v/v, 50 mM NaCl) and the temperature of the column was maintained constant at 25 °C. Samples (500 μM) were prepared in H_2O:MeCN (1:1, v/v) and were analysed in triplicates in three separate experiments (50 μL injection volume). Their capacity factors were calculated using the following equations, where t_R is the retention time of the retained complex, t_0 is the retention time of unretained compound (uracil), R_F is the retention factor, and K is the capacity factor.

$$R_F = (t_R - t_0) \quad (1)$$

$$K = R_F/t_0 \quad (2)$$

2.7. Partition coefficients

Octanol/water partition coefficients (Log $P_{o/w}$) of complexes were determined using an adaptation of the shake-flask method [29,30]. Octanol-saturated water (OSW) and water-saturated octanol (WSO) were prepared by stirring octanol (100 mL) and doubly-deionised water (100 mL) together for 24 h and separating the two layers. Prior to mixing, the water was supplemented with NaX (300 mM), where X = Cl, Br, or I, added to suppress the hydrolysis of chlorido, bromido, or iodido complexes, respectively. Complexes (0.5–3.0 mg) were dissolved in OSW (3 mL) with vigorous stirring/shaking for 24 h, then filtered. Saturated solutions of complexes in OSW (1 mL) were combined with WSO (1 mL) in falcon tubes and placed on a Vibrax VXB basic mechanical shaker for 24 h at 500 g/min. Samples of aqueous phases were collected before and after partitioning and their osmium concentrations were determined by Inductively Coupled Plasma-Mass Spectrometry (ICP-MS) or Inductively Coupled Plasma-Optical Emission Spectroscopy (ICP-OES). Partition coefficients were calculated via Eq. (3). Experiments were performed as duplicates of triplicates in two independent experiments at ambient temperature.

$$\text{Log } P_{o/w} = \text{Log } ([\text{Os}]_{\text{octanol}}/[\text{Os}]_{\text{water}}) \quad (3)$$

2.8. Electrochemistry

Cyclic voltammetry analyses were performed using a CH Instruments Electrochemical Analyzer (CHI420C) and CH Instruments electrochemistry software. Compounds were dissolved in acetonitrile (1 mg/mL) with $^nBu_4NPF_6$ (0.1 M) as a supporting electrolyte. Solutions were degassed under N_2 and scanned between −2.0 V and +2.0 V at scan rates of 0.1 or 0.5 V/s. A three-electrode system was used: a platinum working electrode, a Ag/Ag^+ in $AgNO_3$ (10 mM, MeCN) non-aqueous reference electrode, and a platinum wire counter electrode.

2.9. In vitro growth inhibition assay

Approximately 5000 cells (A2780, MCF-7, SUNE1, OE19 or MRC-5) were seeded per well in 96-well plates. The cells were pre-incubated in drug-free media for 48 h before adding different concentrations of complexes in medium. After 24 h of incubated drug exposure, the supernatants were removed and cells were washed with PBS. The cells were allowed to recover in drug-free medium for 72 h incubation and the sulforhodamine B assay was used to determine cell viability. Absorbance measurements of the solubilised dye (on a BioRad iMark microplate reader using a 470 nm filter) allowed the determination of viable treated cells compared to untreated controls. IC_{50} values (concentration at which 50% cell death occurs) were determined as duplicates of triplicates for each complex. ICP-OES was used to determine the osmium concentrations of the initial stock solutions of complexes in medium, which were used for determination of IC_{50} values.

2.10. Cell uptake

Approximately 4 × 10^6 A2780 cells were seeded into P100 Petri dishes. After 24 h pre-incubation in drug-free medium, complexes were added in equipotent concentrations of $IC_{50}/3$ and the cells incubated for 24 h. The cells were then treated with trypsin, counted, and cell pellets were collected. Control samples were included with untreated cells. Cell pellets were digested overnight in 72% distilled HNO_3 at 80 °C in Wheaton V-vials. The resulting solutions were diluted in a stabilisation solution (10 mM thiourea and 0.1 g/L ascorbic acid), diluting them to 3.6% HNO_3. Ascorbic acid reduces volatile OsO_4 generated during the digestion process and thiourea is an osmium-binding agent [31].

Osmium concentrations were determined by ICP-MS. Measurements were carried out in triplicate for each complex and cellular accumulation was calculated in units of ng Os/10^6 cells.

2.11. ROS assay

Flow cytometry analysis of ROS/superoxide generation in A2780 cells caused by exposure to osmium complexes, was carried out using the Total ROS/Superoxide detection kit (Enzo-Life sciences) according to the supplier's instructions. Briefly, 1.5 × 10^6 cells per well were seeded in a 6-well plate. Cells were pre-incubated in drug-free media for 24 h, then complexes were added to triplicates at 1× and 2× IC_{50}. After 24 h of incubated drug exposure the supernatants were removed and the cells were washed with PBS. Cells were harvested using trypsin and collected after centrifugation. Positive controls (cells treated with pyocyanin) and negative controls (untreated cells) were included in the study. Staining was achieved by re-suspending the cell pellets in buffer containing the orange/green fluorescent reagents. Cells were analysed on a Becton Dickinson FACScan Flow Cytometer using FL1 channel (excitation/emission: 490/525 nm) for the oxidative stress and FL2 channel (excitation/emission: 550/620 nm) for superoxide detection. Compensation adjustments were carried out using pyocyanin-treated cells singly-stained with either fluorescent agent. Data were processed using Flowjo software.

2.12. Cell cycle analysis

Briefly, 1.5 × 10^6 A2780 cells per well were seeded in a 6-well plate. Cells were pre-incubated in drug-free media for 24 h, then complexes were added to triplicates at 1× or 2× IC_{50} concentrations. Control samples with untreated cells were included. After 24 h of incubated drug exposure the supernatants were removed and the cells were washed with PBS, harvested using trypsin, then fixed with 70% ethanol and stored at −20 °C. DNA staining was achieved by re-suspending the cell pellets in PBS containing propidium iodide (PI) and RNase. Cell pellets were re-suspended in fresh PBS before being analysed in a Becton Dickinson FACScan flow cytometer, using excitation of DNA-bound PI at 536 nm with emission at 617 nm. Data were processed using Flowjo software.

2.13. Apoptosis

Flow cytometry analyses of apoptotic populations of A2780 cells caused by exposure to complexes were carried out using the Biovision Annexin V-FITC (fluorescein isothiocyanate) apoptosis detection kit according the supplier's instructions. Briefly, 1.5 × 10^6 cells per well were seeded in a 6-well plate. Cells were pre-incubated in drug-free media for 24 h, then complexes were added to triplicates at 1× and 2× IC_{50} concentrations. Control samples with untreated cells were included. After 24 h of incubated drug exposure, supernatants were removed and cells were washed with PBS. Cells were harvested using trypsin and collected after centrifugation. The cells were stained with Annexin V-FITC and PI and analysed using a Becton Dickinson FACScan flow cytometer, running Cell Quest software (20,000 events were collected from each sample).

3. Results and discussion

3.1. Synthesis

AZPY ligands functionalised with alkoxy or glycolic side-chains (RO-AZPY) were prepared from a ligand we reported previously, 2-(phenylazo)-5-fluoropyridine (5-F-AZPY, Scheme S1) [4]. The synthesis involves an addition-elimination nucleophilic substitution mechanism, where the alcohol/glycol reagent (ROH) behaves as a solvent matrix, and nucleophile, RO^-, is generated in situ under basic conditions, attacking the electropositive fluorinated carbon at the 5-position (Scheme S2). A total of 13 ligands were synthesised, **L1-L13**, utilising a variety of alcohols and glycols with different chain lengths. Table S1 summarises ligands **L1-L13** and the reagents/solvents (ROH) used to generate them.

Twenty-four novel Os(II) arene AZPY complexes were synthesised, where the arene, monodentate ligand (X), counter anion (Y), and ligand substituent (R) were varied (Fig. 1). Complex **5**, [Os(η^6-*p*-cym)(5-EtO-AZPY)I]PF_6, was synthesised previously and its X-ray crystal structure determined [32]. Their syntheses involve stirring osmium dimer, [Os(η^6-arene)X_2]$_2$ (where X = Cl, Br or I and arene = *p*-cym or bip), in ethanolic solution with 2.1 mol. equiv. of ligand (**L1-L13**). The generated cationic complex is then paired with a counter-anion; PF_6^-, $CF_3SO_3^-$, or IO_3^-, by adding either NH_4PF_6, $NH_4CF_3SO_3$ or KIO_3, respectively (Scheme S3). All complexes were characterised by ^{1}H NMR, electrospray ionisation mass spectrometry (ESI-MS) and CHN analysis, and where satisfactory CHN analyses were not obtained, complexes were additionally characterised by ^{13}C NMR. Purity was determined by reverse-phase analytical RP-HPLC and only complexes ≥96% pure were used for further studies. Impure complexes were purified by recrystallisation or automated reverse-phase column chromatography. ESI-MS analysis of complexes acquired in positive ion mode revealed a *m/z* peak corresponding to the cationic species without counter-anion, [M-Y]. In negative mode, a *m/z* peak corresponding to the anion was observed (145.0 and 149.0 for PF_6^- and $CF_3SO_3^-$, respectively, see Fig. S1).

3.2. X-ray crystal structures

The molecular structures of compounds **1** and **8** were determined by X-ray crystallography (Fig. 2 and Table S2). The structures adopt the familiar pseudo-octahedral three-legged piano-stool geometry, where Os(II) is π-bonded to the arene ligand, and coordinated to a monodentate iodido ligand and a bidentate RO-AZPY ligand, which constitute the three legs of the piano-stool. The complexes crystallised as racemates owing to their chiral metal centres, and contain PF_6^- counter-anions in their x-ray crystal structures.

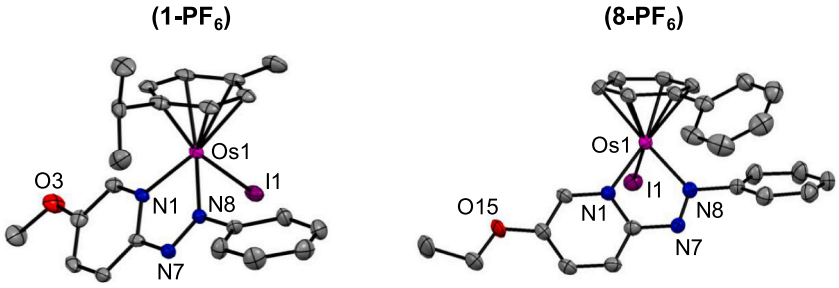

Fig. 2. ORTEP diagrams for the X-ray crystal structures of complexes **1** and **8**. Ellipsoids are shown at the 50% probability level and all hydrogens and counter ions have been omitted for clarity.

3.3. Hydrolysis studies

The extent of hydrolysis of chlorido, bromido, and iodido analogues, [Os(η^6-*p*-cym)(5-EtO-AZPY)Cl]PF_6 (**3**), [Os(η^6-*p*-cym)(5-EtO-AZPY)Br]PF_6 (**4**) and [Os(η^6-*p*-cym)(5-EtO-AZPY)I]PF_6 (**5**), was determined by RP-HPLC for 100 μM solutions after 0, 2, 12 and 24 h at 37 °C. They were solubilised in phosphate buffer (95 mol equiv., pH 7.4, 5% v/v DMSO) and with two concentrations of added NaCl: 23 mM (intracellular conditions) and 103 mM (extracellular conditions). RP-HPLC chromatograms are shown in Fig. S2. Complexes **3** and **4** show significant levels of hydrolysis after 24 h incubation in 23 mM NaCl, with 85% and 84% of the hydroxido species, [Os(η^6-*p*-cym)(5-EtO-AZPY)OH]$^+$ (**3OH**), present, respectively. The previously reported aqua-species has a low pK_a (4.55), indicating that the more stable Os-OH species predominates under physiological conditions over the more labile Os-OH_2 species [32]. Incubation in 103 mM NaCl partially suppresses hydrolysis of **3** and **4**, with 61% and 58% hydrolysis occurring after 24 h, respectively. For bromido complex **4**, formation of the chlorido species is also observed in the presence of NaCl, occurring at 8% and 27%, respectively for 23 mM and 103 mM NaCl. In contrast, the iodido complex **5** is significantly more inert towards hydrolysis, showing only 7% and 4% hydrolysis after 24 h incubation in the presence of 23 mM and 103 mM NaCl, respectively, and only 1% and 2% formation of the chlorido species, respectively. Complexes **3** and **4** exhibit low stability in comparison to previously reported chlorido AZPY complex, [Os(η^6-*p*-cym)(AZPY-NMe_2)Cl]PF_6, which remained inert towards hydrolysis even when heated with 1 mol. equiv. $AgNO_3$ [5]. Interestingly, this complex has sub-micromolar activity against A2780 cells, which may in part be a result of its inherent stability.

3.4. Antiproliferative activity

The IC_{50} values for complexes **2–7** and **9–11**, and **13–24** towards A2780 human ovarian cancer cells were determined and are summarised in Table 1 and Fig. S3. Complexes **1** and **12** were too insoluble in aqueous media to conduct biological assays. However, replacing the PF_6^- counter-anion of **1** with $CF_3SO_3^-$ led to a 45-fold increase in solubility (from 9 to 405 μM maximum solubility in 100 mM $NaCl_{(aq)}$ at 20 °C, Fig. S3), enabling biological evaluation of **2**. Moreover, changing the counter-anion from PF_6^- to $CF_3SO_3^-$ has no major impact on antiproliferative activity, as shown by the similar activities of **5** and **6** (A2780 IC_{50} = 0.92 and 0.9 μM, respectively), which exhibit maximum aqueous solubilities of 52 and 185 μM, respectively. Further trends in aqueous solubility and antiproliferative activity are summarised in the SI.

Table 1
IC_{50} concentrations (μM) for complexes **2–7** and **9–11**, and **13–24** against A2780 human ovarian cancer cells.

A2780 Ovarian cancer cells	
Complex	**IC_{50} (μM)**
(**1**) [Os(η^6-*p*-cym)(5-MeO-AZPY)I]PF_6	n.d.
(**2**) [Os(η^6-*p*-cym)(5-MeO-AZPY)I]CF_3SO_3	0.5(± 0.1)
(**3**) [Os(η^6-*p*-cym)(5-EtO-AZPY)Cl]PF_6	15.1(± 0.5)
(**4**) [Os(η^6-*p*-cym)(5-EtO-AZPY)Br]PF_6	14.1(± 0.9)
(**5**) [Os(η^6-*p*-cym)(5-EtO-AZPY)I]PF_6	0.92(± 0.02)
(**6**) [Os(η^6-*p*-cym)(5-EtO-AZPY)I]CF_3SO_3	0.9(± 0.2)
(**7**) [Os(η^6-*p*-cym)(5-EtO-AZPY)I]IO_3	1.6(± 0.3)
(**8**) [Os(η^6-bip)(5-EtO-AZPY)I]PF_6	n.d.
(**9**) [Os(η^6-bip)(5-EtO-AZPY)I]CF_3SO_3	0.51(± 0.02)
(**10**) [Os(η^6-*p*-cym)(5-^{n}PrO-AZPY)I]PF_6	0.33(± 0.02)
(**11**) [Os(η^6-*p*-cym)(5-^{i}PrO-AZPY)I]PF_6	0.30(± 0.09)
(**12**) [Os(η^6-*p*-cym)(5-^{n}BuO-AZPY)I]PF_6	n.d.
(**13**) [Os(η^6-*p*-cym)(5-HOCH_2CH_2O-AZPY)Cl]PF_6	> 100
(**14**) [Os(η^6-*p*-cym)(5-HOCH_2CH_2O-AZPY)Br]PF_6	> 100
(**15**) [Os(η^6-*p*-cym)(5-HOCH_2CH_2O-AZPY)I]PF_6	20.7(± 0.1)
(**16**) [Os(η^6-bip)(5-HOCH_2CH_2O-AZPY)I]PF_6	2.37(± 0.09)
(**17**) [Os(η^6-*p*-cym)(5-HO{CH_2CH_2O}$_2$-AZPY)I]PF_6	2.04(± 0.06)
(**18**) [Os(η^6-*p*-cym)(5-MeO{CH_2CH_2O}$_2$-AZPY)I]PF_6	1.80(± 0.09)
(**19**) [Os(η^6-*p*-cym)(5-EtO{CH_2CH_2O}$_2$-AZPY)I]PF_6	0.68(± 0.03)
(**20**) [Os(η^6-bip)(5-EtO{CH_2CH_2O}$_2$-AZPY)I]CF_3SO_3	1.9(± 0.2)
(**21**) [Os(η^6-*p*-cym)(5-HO{CH_2CH_2O}$_3$-AZPY)I]PF_6	12(± 1)
(**22**) [Os(η^6-*p*-cym)(5-MeO{CH_2CH_2O}$_3$-AZPY)I]PF_6	2.1(± 0.2)
(**23**) [Os(η^6-*p*-cym)(5-EtO{CH_2CH_2O}$_3$-AZPY)I]PF_6	2.6(± 0.4)
(**24**) [Os(η^6-*p*-cym)(5-HO{CH_2CH_2O}$_4$-AZPY)I]PF_6	7.6(± 0.6)

Seven complexes (**2**, **5**, **6**, **9**, **10**, **11** and **19**) exhibited sub-micromolar activity against A2780 cells and five were selected for further evaluation against MCF-7 breast cancer, SUNE1 nasopharyngeal cancer, OE19 oesophageal cancer, and MRC-5 lung fibroblast cells (Table 2). Their selectivity factors (SF) towards cancer cells over normal cells were calculated as a ratio of IC_{50}(MRC-5)/IC_{50}(A2780). With the exception of **19**, complexes screened against SUNE1 cells show highly potent sub-micromolar activity. Complexes **5**, **9** and **19** exhibit exceptionally potent activity against OE19 cells with **9** exhibiting low nanomolar potency (96 nM), whilst **11** exhibits the highest activity against A2780 cells, comparable to other complexes reported in its class [4,5]. In contrast, these complexes are generally less active against MCF-7 cells, with the highest activity observed for **5** (1.2 μM). Overall, complex **9** displays the broadest anticancer profile amongst all the tested cell lines and the highest SF; comparable with that of cisplatin [14].

3.5. Capacity factor and correlation with antiproliferative activity

The capacity factor (*K*) of a compound is related to its RP-HPLC retention time and is independent of column geometry and mobile phase flow rate. It serves as a measure of affinity towards a hydrophobic stationary phase versus an aqueous mobile phase, hence providing a measure of relative lipophilicity [33,34]. The higher the *K*-value of a compound, the greater its lipophilicity. The *K*-values of complexes **2–6** and **9–24** were determined by RP-HPLC using a C18 column and isocractic mobile phase of MeCN:H_2O (1:1, v/v, 50 mM NaCl), and are shown in Fig. S3. Trends in the capacity factors of these complexes are discussed in the SI, and correlations between antiproliferative activity towards A2780 cells and capacity factor are shown in Fig. 3. Inverse correlations are observed; i.e. when relative lipophilicity increases, the IC_{50} value generally decreases (increased activity), which is overall likely due to the improved cellular accumulation of complexes exhibiting higher lipophilicity. This was investigated by examining correlations where specific substituents are varied.

When the monodentate halido ligand (X) is varied, a strong inverse correlation between activity and relative lipophilicity is observed (−0.96, Fig. 3a). Complexes with monodentate iodido ligands are considerably more active than their chlorido and bromido counterparts, with the observed trend: I ≫ Br ≥ Cl. The same trend was observed previously for other Os(II) AZPY complexes [4]. The improved stability of iodido complexes may account for their increased activity as they are less likely to be deactivated by extracellular side reactions. Using ^{131}I radio-labelling, we showed previously that iodido complex **5** is stable in extracellular conditions and activated via monodentate ligand loss in MCF-7 breast cancer cells [32]. Likewise, the same trend in *K* is observed: I > Br > Cl, where iodido complexes exhibit the highest lipophilicity, owing to their lower polarisation and more covalent character of the Os-X bond. For complexes containing alkoxy substituents (R) on their AZPY ligand, a weaker correlation between activity and relative lipophilicity is observed (−0.55, Fig. 3b). Increasing the length of this hydrophobic substituent increases *K* (hence relative lipophilicity) in the order: ^{n}Pr > ^{i}Pr > Et > Me. However, activity follows a different trend: ^{i}Pr > ^{n}Pr > Me > Et, that cannot be explained solely by capacity factors.

Moderate correlation was observed between activity and relative lipophilicity for complexes bearing glycolic side-chains, where the length of the glycol (n) was varied and where R* = H (−0.69, Fig. 3c). Varying n does

Table 2
IC_{50} concentrations (μM) for complexes **5**, **9**, **11**, **18**, and **19**, against various cancer cell lines and normal MRC-5 cells. Selectivity factors (SF) are calculated as the ratio IC_{50}(MRC-5)/IC_{50}(A2780).

	Cell line (IC_{50}/μM)				
Complex	**MCF-7**	**SUNE1**	**OE19**	**MRC-5**	**SF**
5	1.2(± 0.2)	0.86(± 0.06)	0.20(± 0.03)	2.2(± 0.2)	2.4
9	15(± 2)	0.31(± 0.02)	0.096(± 0.004)	6.1(± 0.1)	12.0
11	7.1(± 0.2)	n.d.	n.d.	1.99(± 0.07)	6.6
18	10(± 1)	n.d.	n.d.	7.4(± 0.8)	4.1
19	12.9(± 0.8)	1.7(± 0.1)	0.42(± 0.01)	3.6(± 0.3)	5.3

not appear to have a significant effect on the relative lipophilicity of the complex, possibly because each unit increase in the glycol chain introduces an additional ethereal oxygen capable of H-bonding with water. Likewise, there is no clear trend in activity, which follows the pattern: n = 2 > 4 > 3 > 1. In contrast, when the terminal group on the glycol side-chain (R*) is varied, a strong correlation between activity and relative lipophilicity is observed (−0.90, Fig. 3d). As expected, the trend in *K* follows: Et > Me > H, where complexes with longer hydrophobic groups are more lipophilic. This trend is mirrored by activity, likely due to elevated cell uptake resulting from higher lipophilicity.

3.6. Octanol/water partition coefficients

Octanol/water partition coefficients ($P_{o/w}$) of complexes were measured using a modified version of the shake-flask method [6,29,30,34], where OSW contained 300 mM of NaX (X = Cl, Br or I) to suppress the hydrolysis of chlorido, bromido and iodido complexes, respectively, and complexes were prepared as saturated solutions in OSW prior to the addition of WSO. Without the addition of NaX, potential aqua-adduct formation would complicate the interpretation of data. We generally observed a decrease in complex solubility upon

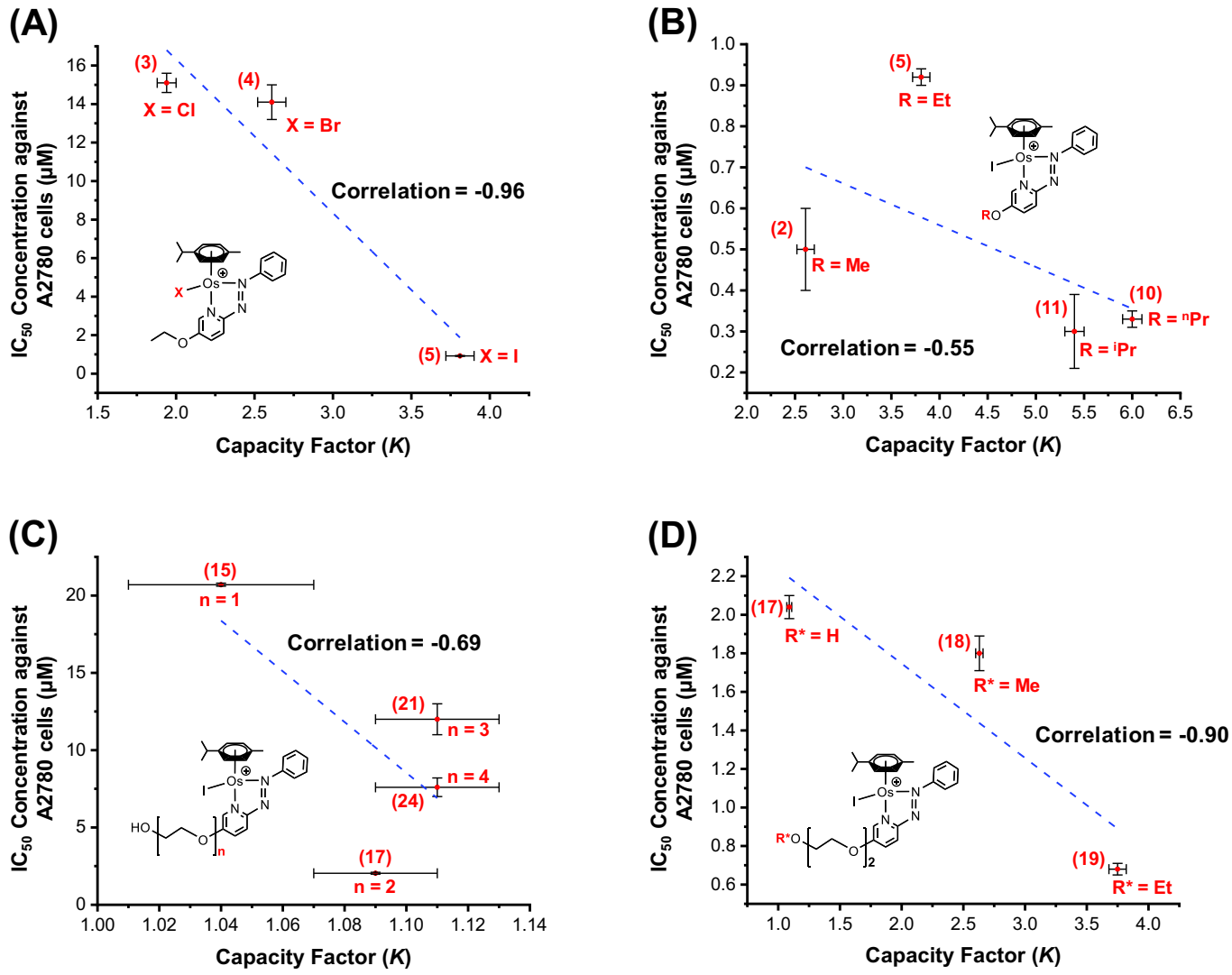

Fig. 3. Correlations between antiproliferative activity (IC_{50} towards A2780 cells, μM) and capacity factor (*K*), where different substituents on the complexes are varied; (A) monodentate halido ligand, X, (B) alkoxyl side-chain substituent, R, (C) length of glycolic side-chain substituent, n, and (D) terminal group of glycolic side-chains, R*.

Table 3
Log *K* values for complexes **2–6** and **9–24**, their derived Log P_{HPLC} values, and Log $P_{o/w}$ values for complexes **4**, **13**, **15**, **16**, **18**, **19** and **21** measured using a modified shake-flask method.

Complex	Log (*K*)	Log ($P_{o/w}$)	Log (P_{HPLC})
2	0.42(± 0.02)	n.d.	2.1(± 0.5)
3	0.29(± 0.01)	n.d.	1.8(± 0.4)
4	0.42(± 0.01)	1.59(± 0.03)	2.1(± 0.5)
5[a]	0.58(± 0.01)	n.d.	2.5(± 0.6)
6[a]	0.60(± 0.01)	n.d.	2.6(± 0.6)
9	0.56(± 0.01)	n.d.	2.5(± 0.6)
10[a]	0.779(± 0.009)	n.d.	3.0(± 0.7)
11[a]	0.733(± 0.008)	n.d.	2.9(± 0.7)
12[a]	0.972(± 0.007)	n.d.	3.5(± 0.8)
13	−0.25(± 0.02)	0.11(± 0.02)	0.6(± 0.4)
14	−0.13(± 0.02)	n.d.	0.8(± 0.3)
15	0.02(± 0.02)	1.87(± 0.05)	1.2(± 0.2)
16	0.00(± 0.03)	1.10(± 0.04)	1.1(± 0.2)
17	0.038(± 0.009)	n.d.	1.2(± 0.2)
18	0.420(± 0.005)	2.29(± 0.04)	2.1(± 0.5)
19	0.574(± 0.007)	2.6(± 0.2)	2.5(± 0.6)
20	0.548(± 0.007)	n.d.	2.4(± 0.5)
21	0.044(± 0.007)	1.41(± 0.04)	1.3(± 0.2)
22	0.402(± 0.006)	n.d.	2.1(± 0.5)
23	0.555(± 0.006)	n.d.	2.5(± 0.6)
24	0.045(± 0.007)	n.d.	1.3(± 0.2)

[a] Log (*K*) value outside the calibration range.

addition of NaX to aqueous media (salting-out effect) [35]. To gain a full understanding on the salt effect on Log $P_{o/w}$ for our complexes, further experiments at fixed concentrations would be required [36]. In general, increasing the ionic strength of OSW tends to increase Log $P_{o/w}$ values for lipophilic compounds [37]. Log $P_{o/w}$ was determined for selected complexes (**4**, **13**, **15**, **16**, **18**, **19** and **21**), as it was not possible to make measurements on complexes with very poor aqueous solubility due to the limit of Os detection via ICP-MS after partitioning.

An alternative RP-HPLC method for determining Log P_{HPLC} was adopted; using the *K*-values, a calibration curve of Log $P_{o/w}$ vs. Log *K* was plotted for complexes **4**, **13**, **15**, **16**, **18**, **19** and **21** [38] (Fig. S4), and Log P_{HPLC} values for all complexes were derived (Table 3). Due to relatively weak correlation (+0.743), the Log P_{HPLC} values have notable error margins, but are suitable enough for these purposes of comparison. The Log *K* values of **5**, **6** and **10–12** fall outside the range of the calibration plot and their Log P_{HPLC} values were estimated by extrapolating the curve. All determined Log P_{HPLC} values fall well within the Ro5 range (−0.4 to +5.6). Following an approach outlined by Sahu et al, Log $P_{o/w}$ was plotted on the x-axis as a reference indicator against the expression Log ($K/P_{o/w}$) to determine whether factors other than lipophilicity contribute towards partitioning, i.e. chemical interactions with solvents, such as hydrolysis [38]. The plot shows a strong correlation (+0.935), indicating that partitioning of the complexes is largely determined by lipophilicity (Fig. S5).

3.7. Cellular accumulation

The cellular accumulation of Os in A2780 cells was determined for complexes **2–6**, **9** and **13–15**, by ICP-MS (Fig. 4). Trends between **3** and **5** and **13–15** show that iodido complexes promote greater accumulation of Os than their chlorido and bromido analogues, and the same trend is observed for anticancer activity: I > Br > Cl. The enhanced activity and accumulation of iodido complexes inside cells is likely to be due in part to increased lipophilicity, as well as their improved stability. The trend between **5** and **6** shows that anions have little effect on cellular accumulation, activity and lipophilicity, due to their lack of role once complexes are solvated in medium. Switching the arene from *p*-cym to bip decreases cellular accumulation and lipophilicity, as shown by the trend between **6** and **9**. Interestingly, this change also led to an improvement in anticancer activity, which may be due to factors other than lipophilicity. When the R-substituent is varied, the trend in cell uptake follows the same order as lipophilicity: Et > Me > $HOCH_2CH_2$, as observed for complexes **2**, **5**, **6** and **15**. Overall, reasonably strong correlation is observed between cellular accumulation and *K*-value for complexes **2–6**, **9** and **13–15** (+0.78), thus indicating a linear trend between the lipophilicity of this series of complexes and their ability to accumulate in cancer cells (Fig. S6).

3.8. Cyclic voltammetry

The electrochemistry of complexes **2**, **3**, **5**, **9–11**, **15**, **18**, **19**, and ligand **L2** in MeCN was investigated by cyclic voltammetry. Complexes **2**, **5**, **9**, **11**, and **19** were scanned between +2.0 to −2.0 V and notable redox activity was observed between +0.5 to −1.5 V (Fig. S7). All complexes exhibit two reductions between 0.0 to −2.0 V, assignable to irreversible reductions of the azo-bond [39] (Figs. 5, S8 and Scheme S4). However, upon scanning from 0.0 to −1.0 V, chlorido complex **3** exhibits a reversible first reduction potential, in contrast to its iodido anologues, all of which were irreversible. Interestingly, the first reduction of **3** was reversible only when the azo-bond did not undergo a second e^- transfer, suggesting irreversible chemical changes to the structure occur once the azo-bond is fully reduced. Furthermore, second segments in the voltammograms for **5** and **9** show oxidation potentials (−0.35 and −0.31 V, respectively) not corresponding to reversal of their first azo-bond reductions. Hence implying that irreversible chemical changes to iodido complexes can occur after the first azo-bond reduction.

In summary, the first and second azo-bond reductions of these complexes range between −0.75 to −0.79 and −1.27 to −1.63 V, respectively (Table S3). Ligand **L2**, which is present in complexes **3**, **5**, and **9**, exhibits only one reversible reduction at −1.73 V. In comparison to previously reported complexes, this series has lower potentials for their first azo-bond reductions. The reductions of parent complex [Os(η^6-*p*-cym)(AZPY-NMe_2)I]PF_6 (FY026), and its Ru analogue, [Ru(η^6-*p*-cym)(AZPY-NMe_2)I]PF_6, were previously determined as −0.64 and −0.40 V, respectively. Both are notably higher and the latter falling within the biologically relevant region [40].

3.9. Induction of ROS

Complexes **2**, **5**, **9**, **11**, and **19** were screened for ROS induction in A2780 human ovarian cancer cells using flow cytometry. The protocol utilises a total ROS/Superoxide detection kit capable of distinguishing $O_2\cdot^-$ from other ROS. The positive control was treated with pyocyanin and showed the majority of cells expressing high levels of ROS/$O_2\cdot^-$, and the negative control was untreated cells. Figs. 6 and S9 show quantitatively the elevation of ROS after incubation with **2**, **5**, **9**, **11**, and **19** at 1× and 2× IC_{50}. In every case, significantly elevated levels of ROS and $O_2\cdot^-$ were observed, thus further highlighting that the mechanism of action for this class of Os(II) complexes involves generating oxidative stress in cancer cells [5,6,14,40]. Interestingly, **5** and **19** both elevated cellular levels of $O_2\cdot^-$ when their concentrations were doubled, as shown by significant increases in the populations of cells in quadrant Q2. Complexes **3**, **5** and their intracellularly generated hydroxido analogue, [Os(η^6-*p*-cym)(5-EtO-AZPY)OH]$^+$ (**3OH**), were also previously reported to generate the highly reactive hydroxyl radical (OH·) upon catabolising H_2O_2 [32]; a comparatively weak ROS that is over-produced in cancer cells [41–43]. Hydroxyl radicals cause damage to cellular lipids, proteins and compartments, leading to cell death [44] and the ability of the complexes studied here to produce both $O_2\cdot^-$ and OH· under physiological conditions likely plays a role in inducing oxidative stress in cancer cells.

3.10. Cell cycle analysis

Changes in the cell cycle phase distribution for A2780 cells after

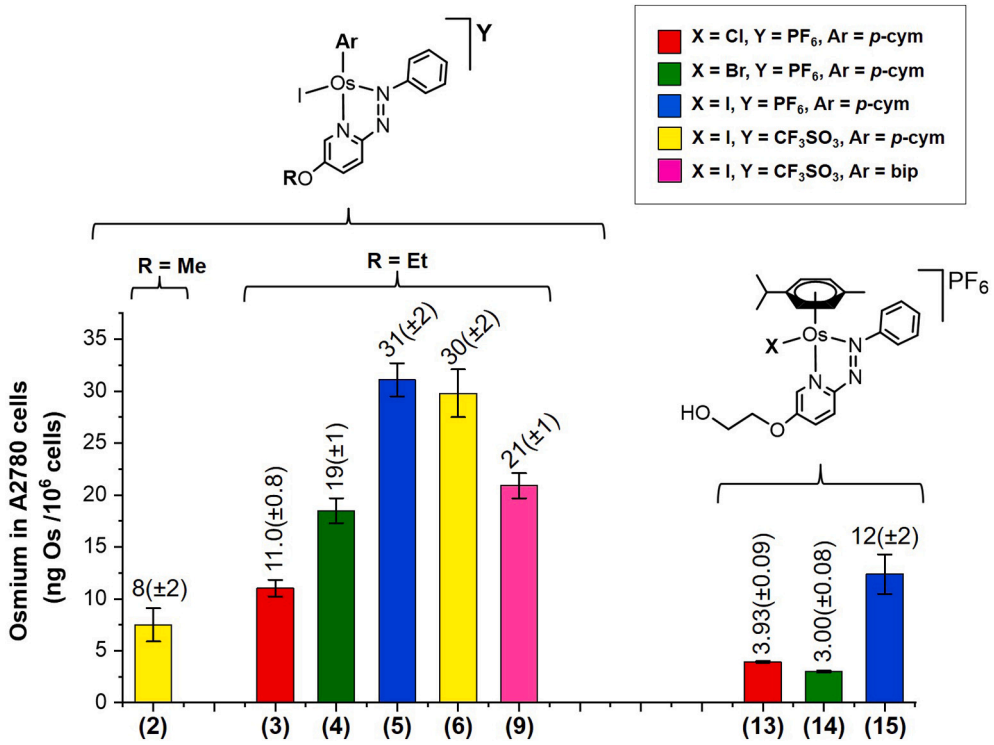

Fig. 4. Trends in cellular Os accumulation for complexes **2–6**, **9** and **13–15** in A2780 cells after treatment with IC_{50}/3 concentration of complex for 24 h.

incubation with sub-micromolar active complex **5**, and less active **15** were monitored using flow cytometry (Figs. 7 and S10). Complex **15** is analogous to **5**, whereby its terminal OH group situated on the ethoxy substituent is deactivating towards anticancer activity but has a strong solubilising effect (Fig. S3a). At 1× IC_{50}, complex **5** causes S-phase cell cycle arrest with an observable decline in the proportion of cells in G1 phase, and at 2× IC_{50}, a rise in the proportion of sub-diploid cells is present. These are damaged non-viable cells with compromised membranes and leakage of their DNA content. In contrast, **15** causes slight elevations in both the G1 and S-phase populations at 1× IC_{50} alongside a small observable decline in the G2/M-phase population. Doubling the concentration induces a large presence of sub-diploid cells, which come primarily from the G1-phase. Such variations in cell cycle effects may arise from differences in AZPY substituents and their subsequent electronic properties.

3.11. Apoptotic behaviour

Complexes **2**, **5**, **9**, **11**, **15** and **19** were screened for their ability to induce apoptosis in A2780 cells, using flow cytometry. Apoptosis is a highly regulated process of programmed cell death which is triggered when cells become damaged or unhealthy. Early stages of apoptosis involve cell shrinkage and blebbing of the cell membrane, whilst later stages involve breakdown of the cellular components/DNA content, and the formation of smaller apoptotic bodies, which are removed from the body by macrophages (Fig. S11). The induction of apoptosis caused after 24 h incubation with **5** and **15** at 1×, 2× and 3× IC_{50}, is shown in Fig. 8. At 2× IC_{50}, **5** and **15** raise the proportion of cells in late-stage apoptosis (Q2) to 22.5% and 5.7%, respectively, and the proportion of non-viable cells (Q1) rises to 40.9% and 17.6%, respectively. At 3× IC_{50}, the proportions of cells in late-stage apoptosis did not significantly increase further, however, greater proportions of non-viable cells were observed; 68.5% and 74.7% for **5** and **15**, respectively. A high presence of non-viable cells suggests the main mechanism of cell death might involve unregulated processes such as necrosis. Complexes **2**, **9**, **11** and **19** were screened at 1× and 2× IC_{50}, however, no significant increase in the proportions of cells in Q3, Q2 or Q1 was observed (Fig. S12).

3.12. NCI-60 data

Complexes **5**, **10** and **15** were evaluated at a 10 μM dose by the National Cancer Institute (NCI) – Developmental Therapeutics Program in their panel of 60 cancer cell lines. Complexes **5** and **10** (mean growths; −48.21% and −52.27%, respectively) inhibit cell growth far more effectively than **15** (mean growth; +88.72%), and are particularly effective against melanoma, inhibiting the growth of all melanomas tested in the study by −75% to −100%. In contrast, other cell types show more varied profiles of growth inhibition when dosed with **5** and **10** (Fig. S13). Complexes **5** and **10** were selected for five-dose response evaluation and their mean GI_{50} values are both 0.42 μM (ca. 3.6× more active than cisplatin). Fig. 9 shows the difference in Log GI_{50} from the mean for **5** and **10** in the 60-cell line panel. Both complexes share a similar trend in activity across the panel, however **5** has a slightly broader range of activity than **10** (0.12–65 μM versus 0.12–30 μM). Both complexes exhibit highest activity against COLO205 colon cancer and lowest activity against NCI/ADR-RES ovarian cancer.

3.13. COMPARE analysis

Complexes **5** and **10** were investigated using the COMPARE algorithm, which produces a linear correlation coefficient to express the level of similarity between two datasets. COMPARE calculations were conducted using methods previously outlined by Zhou et al [45]. The high correlation coefficient determined between the datasets of **5** and **10** (+0.951) suggests they have a common mechanism of action, in keeping with their strong structural similarities. However, there is no correlation of the patterns of activity of **5** and **10** with cisplatin, (correlation coefficients; −0.268 and −0.267, respectively), indicating a different mechanism of action. The COMPARE algorithm was used to compare the 'seed' datasets of **5** and **10** with data from the 'synthetics' database of growth inhibition data for 38,000 synthetic and natural compounds, and the 'standard' database which comprises of 175

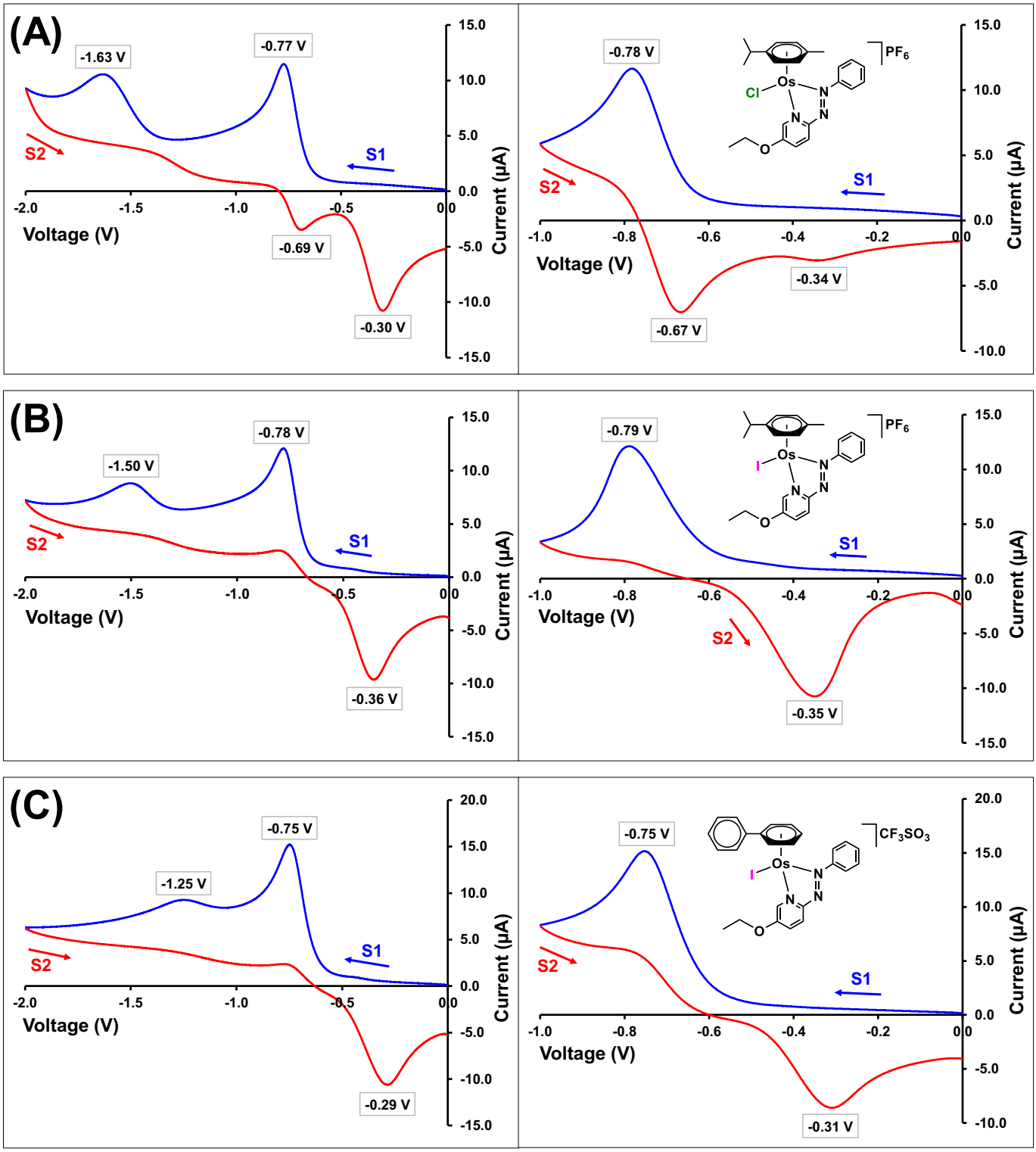

Fig. 5. Cyclic voltammograms for complexes **3** (A), **5** (B), and **9** (C) in MeCN with 0.1 M Bu_4NPF_6 as supporting electrolyte. Complexes were scanned between 0.0 to −2.0 V (left hand side) and 0.0 to −1.0 V (right hand side), and back at 0.1 V/s. The blue and red lines represent the first and second segments, respectively. (For interpretation of the references to colour in this figure legend, the reader is referred to the web version of this article.)

compounds shown to have anti-cancer activity in clinical trials [46]. The COMPARE analyses for the 'synthetics' database in Table 4 display the strongest correlation results for **5** and **10** with Olivomycin and Phyllanthoside, Pearson's correlation coefficients of +0.865 and +0.849, and +0.826 and +0.8470, respectively. Olivomycin has a mechanism of action involving formation of adducts with DNA, leading to the inhibition of RNA synthesis [47], and Phyllanthoside resembles a tRNA, enabling it to inhibit ribosomes and protein synthesis [48]. We reported previously that parent complex, FY026 (analogous to **5** and **10**), shares a similar correlation with Phyllanthoside [49]. Similarly, Bouvardin inhibits protein synthesis by inhibiting 80S ribosomes and also correlates strongly with **5** and **10** [50]. Interestingly, Gamitrinib-

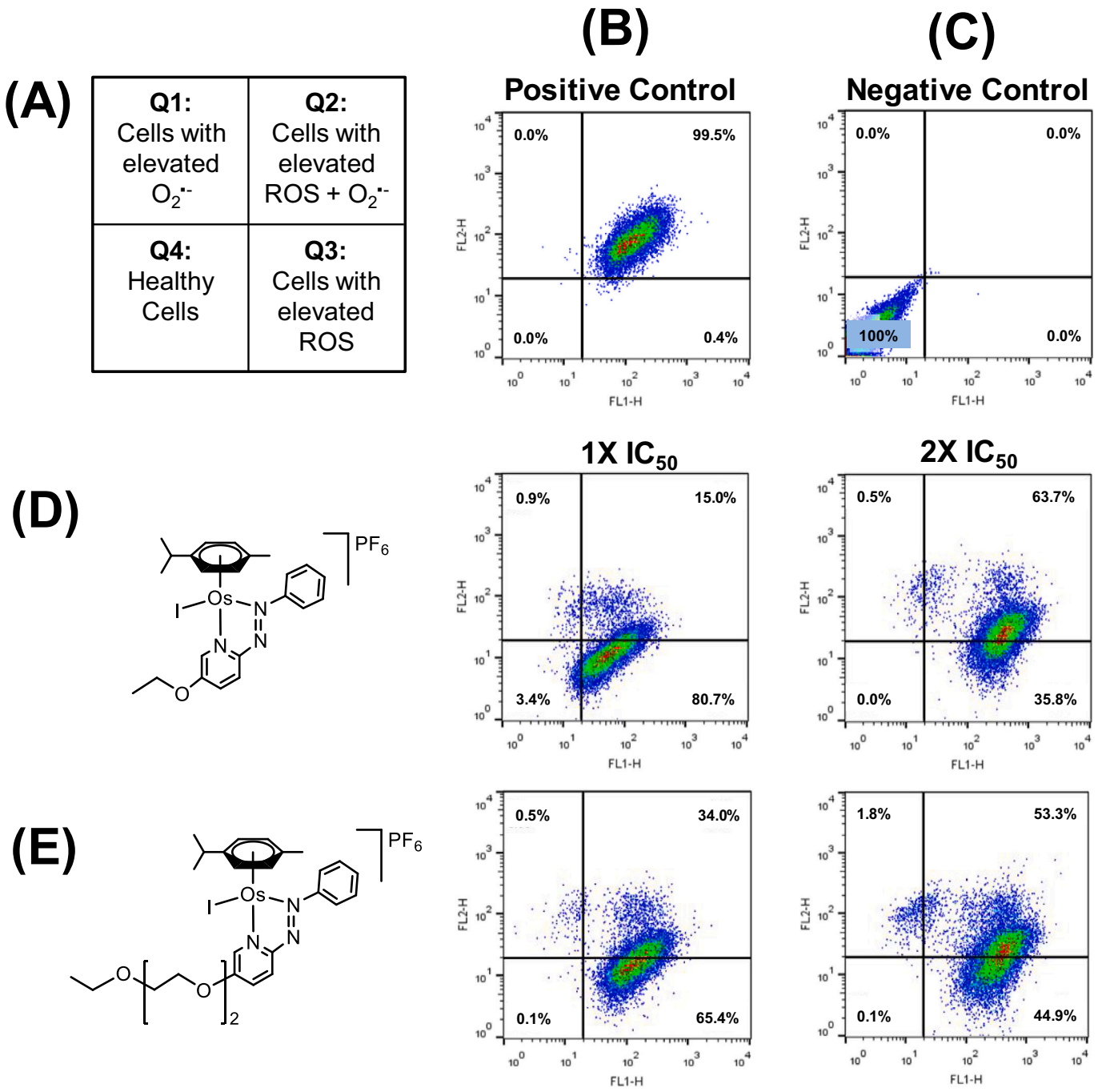

Fig. 6. (A) Diagram showing the four quadrants in the cell population plots; Q1 = cells with elevated levels of superoxide, Q2 = cells with elevated levels of ROS and superoxide, Q3 = cells with elevated levels of ROS, and Q4 = healthy cells. The populations of A2780 cells after 24 h incubation at 37 °C with; (B) pyocyanin (positive control), (C) no drug added (negative control), (D) various concentrations of **5** (1× and 2× IC_{50}), and (E) various concentrations of **19**.

TPP, a mitochondria-targeted Hsp90 inhibitor, also shows high correlation with **5** and **10** (correlation coefficients +0.816 & +0.867, respectively) [51]. Previously, the analogue FY026 was reported to cause altering of the potential across the mitochondrial membrane in A2780 and A549 cancer cells, leading to mitochondrial dysfunction [6,14]. Comparison with compounds in the 'standard' database highlighted resemblance to Chromomycin A3, an inhibitor of RNA polymerase, with correlation coefficients of +0.768 and +0.771 for **5** and **10**, respectively [52].

4. Conclusions

Although about 50% of current chemotherapeutic treatments for cancer involve a platinum drug, there is increasing interest in the discovery of active complexes of other transition metals on account of the need to circumvent resistance to platinum, which is now a clinical problem, and reduce unwanted side-effects. Organometallic complexes offer the possibility of new and unusual mechanisms of action [53–55] and, although not yet widely explored, half-sandwich organo-osmium complexes in particular show promise [56–63].

Here a total of 24 novel complexes (including **5**, which was previously reported) have been synthesised to explore the effect of alkoxy/

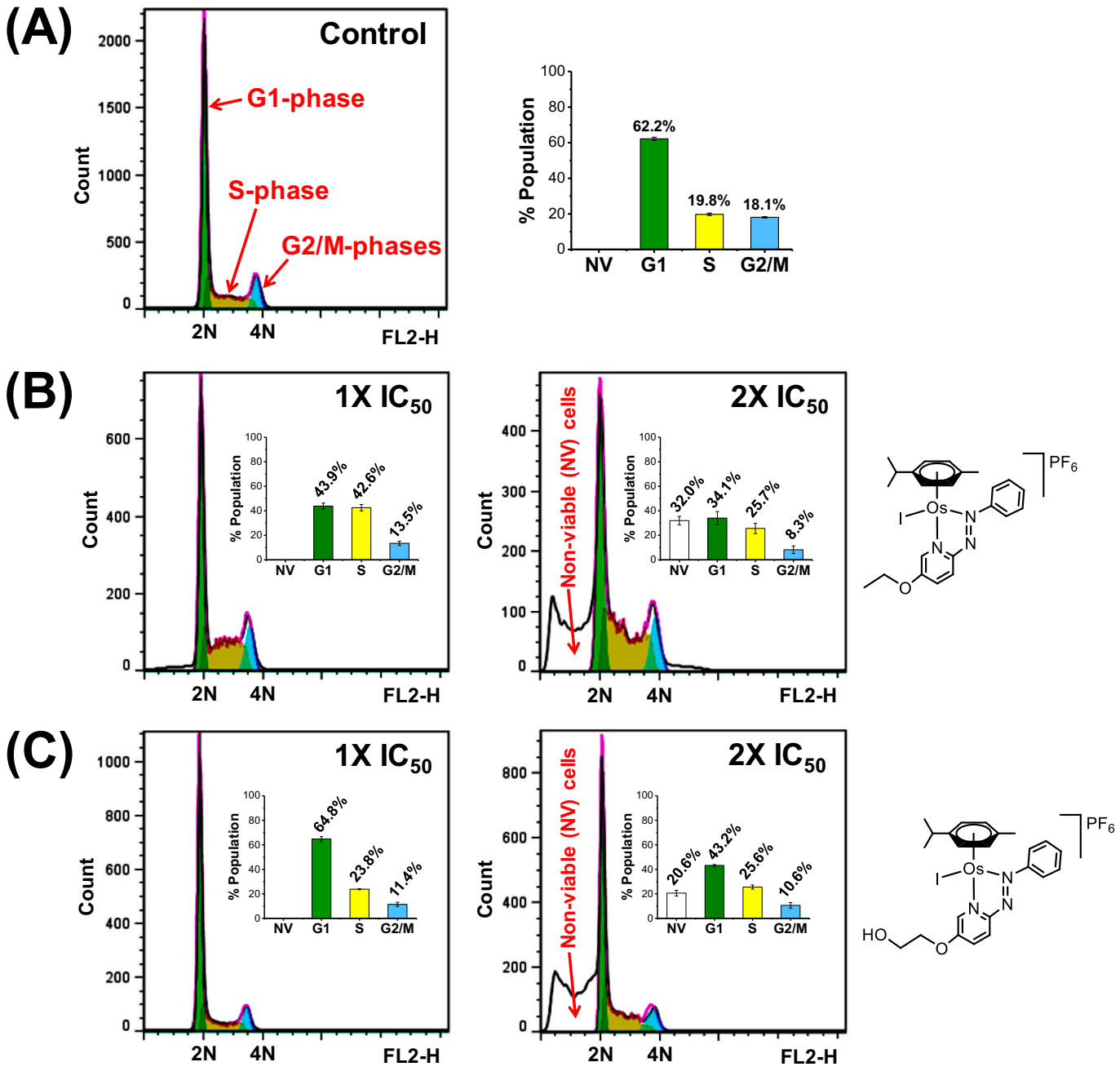

Fig. 7. Flow cytometry data showing cell cycle distributions for A2780 cells after 24 h incubation at 37 °C. (A) Untreated cells (control), and cells treated with (B) **5** and (C) **15** at 1× and 2× IC_{50} concentrations.

glycolic azopyridine substituents on the chemical and anticancer properties of Os(II) arene AZPY complexes. X-ray crystal structures were determined for **1** and **8**. Seven complexes exhibited potent sub micro-molar activity against A2780 human ovarian cancer cells, and five were further screened against other cancer cell lines (MCF-7, SUNE1, OE19) and a normal cell line (MRC-5). Complex **9**, [Os(η^6-bip)(5-EtO-AZPY)I]CF_3SO_3, exhibited the most promising activity profile with extremely potent activity against the oesophageal OE19 cancer cell line (IC_{50} = 96 nM), and the highest selectivity, SF = 12.0, comparable to that of cisplatin. In the NCI-60 panel of cancer cell lines, **5** and **10** exhibited a mean GI_{50} of 0.42 μM, (3.6× more active than *cis*platin), and the COMPARE algorithm showed that the activity of **5** and **10** correlates strongly with one another but poorly with cisplatin, indicating that they have a different mechanism of action, and therefore may overcome platinum resistance, a current clinical problem.

The SARs were explored for anticancer activity, aqueous solubility, capacity factor, and cell uptake (summarised in Fig. S14). The most notable SAR occurs when the halido ligand is varied; anticancer activity follows a distinct trend (I ≫ Br > Cl), which correlates with lipophilicity and cell uptake, but solubility follows the opposite trend. Iodido complexes are considerably more active, largely owing to their enhanced stability [32]. Furthermore, their elevated lipophilicity is likely responsible for increased cellular accumulation (and hence in part improved activity), but also their notable reduction in solubility. Likewise, the same SARs are observed when R* is varied on the complexes bearing glycolic substituents, where activity follows Et > Me > H. Interestingly, complexes bearing bip arenes are generally more active than their *p*-cym counter-parts, however they are much less soluble and

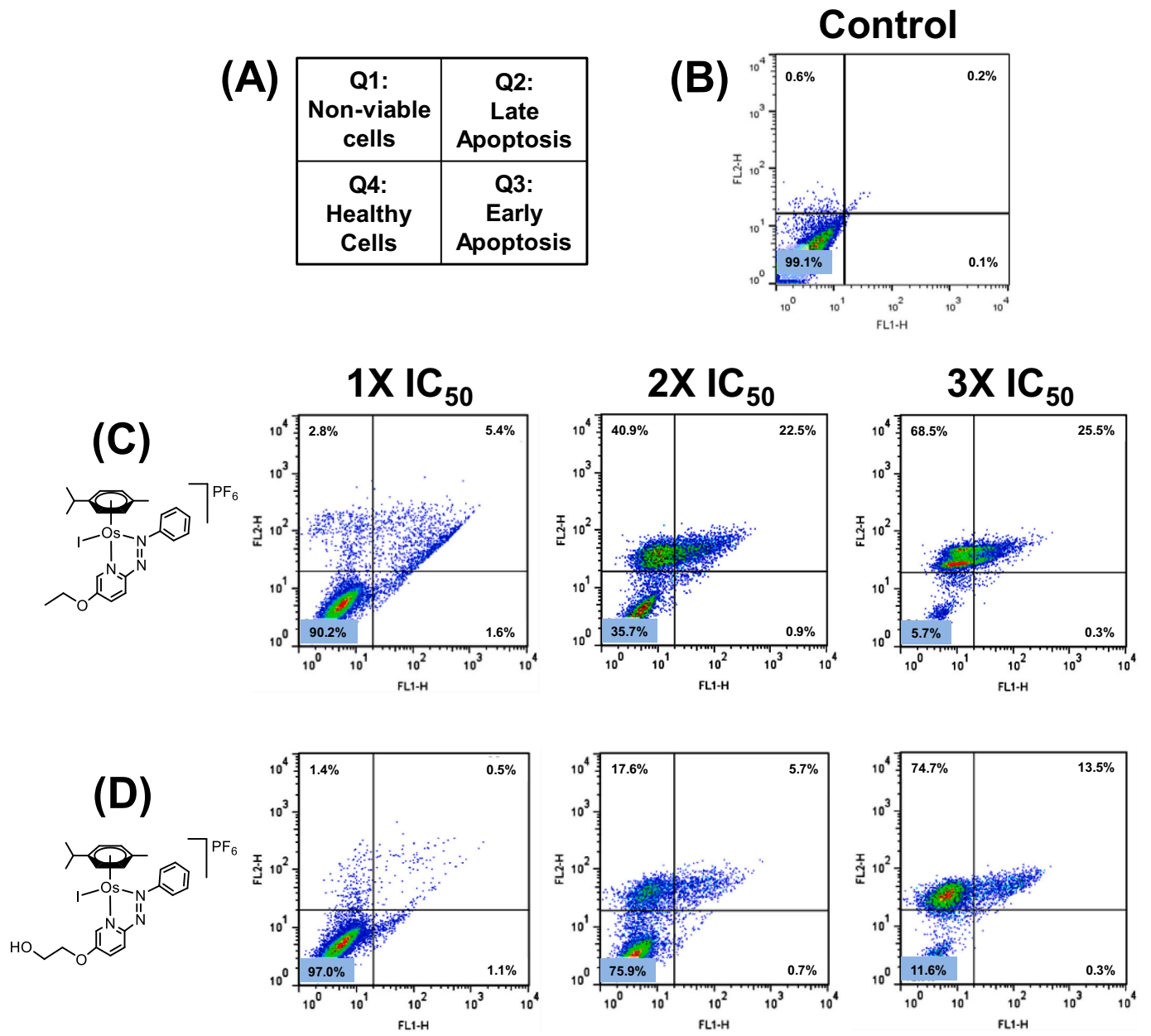

Fig. 8. (A) Diagram representing the four quadrants in cell population plots; Q1 = non-viable cells, Q2 = late-stage apoptotic cells, Q3 = early-stage apoptotic cells, and Q4 = healthy cells. The populations of A2780 cells after 24 h incubation at 37 °C for; (B) untreated cells (control), (C) cells treated with **5**, and (D) **15** at 1×, 2× and 3× IC_{50} concentrations.

slightly less lipophilic, resulting in reduced cellular accumulation. The observed improvement in activity must be due to factors other than greater cell uptake, perhaps the potential for extended arenes to be involved in hydrophobic interactions [64]. An important aim was to improve complex solubility without drastically affecting activity, to facilitate ease of formulation for possible clinical administration. Two strategies were particularly effective: varying the anion (Y), and changing the substituent (R) to a branched equivalent (c.f. **10** and 5× more soluble **11**, which have substituents ^{n}Pr and ^{i}Pr, respectively) [65]. Both strategies involve lowering crystal packing energies, with the former being more effective. As expected, counter-anions play no major role in activity, hence large increases in solubility can be achieved without adversely affecting activity or lipophilicity.

These complexes exhibit reduction potentials corresponding to two electron transfers into the π* orbital of the azo-bond, the first of which falls close to the biologically relevant range of potentials, indicating they may be reducible in cells. The azo-bond is likely to mediate redox reactions in cancer cells, leading to elevated ROS. Consequently, complexes **2**, **5**, **9**, **11**, and **19** are capable of elevating ROS and $O_2\cdot^-$ levels in A2780 ovarian cancer cells. Complexes **5** and **15** also increased the proportion of cells in late-stage apoptosis. However, apoptosis may not be the primary mechanism of cell death as even higher proportions of non-viable cells were observed. Furthermore, **5** and **15** were capable of inducing cell cycle arrest in different phases of the cell cycle: **5** induced S-phase arrest, whilst **15** slightly elevated the proportion of cells in G1-phase. These effects could play a role in reducing the proliferation of cancer cells, and highlights potential mechanistic differences between structural analogues.

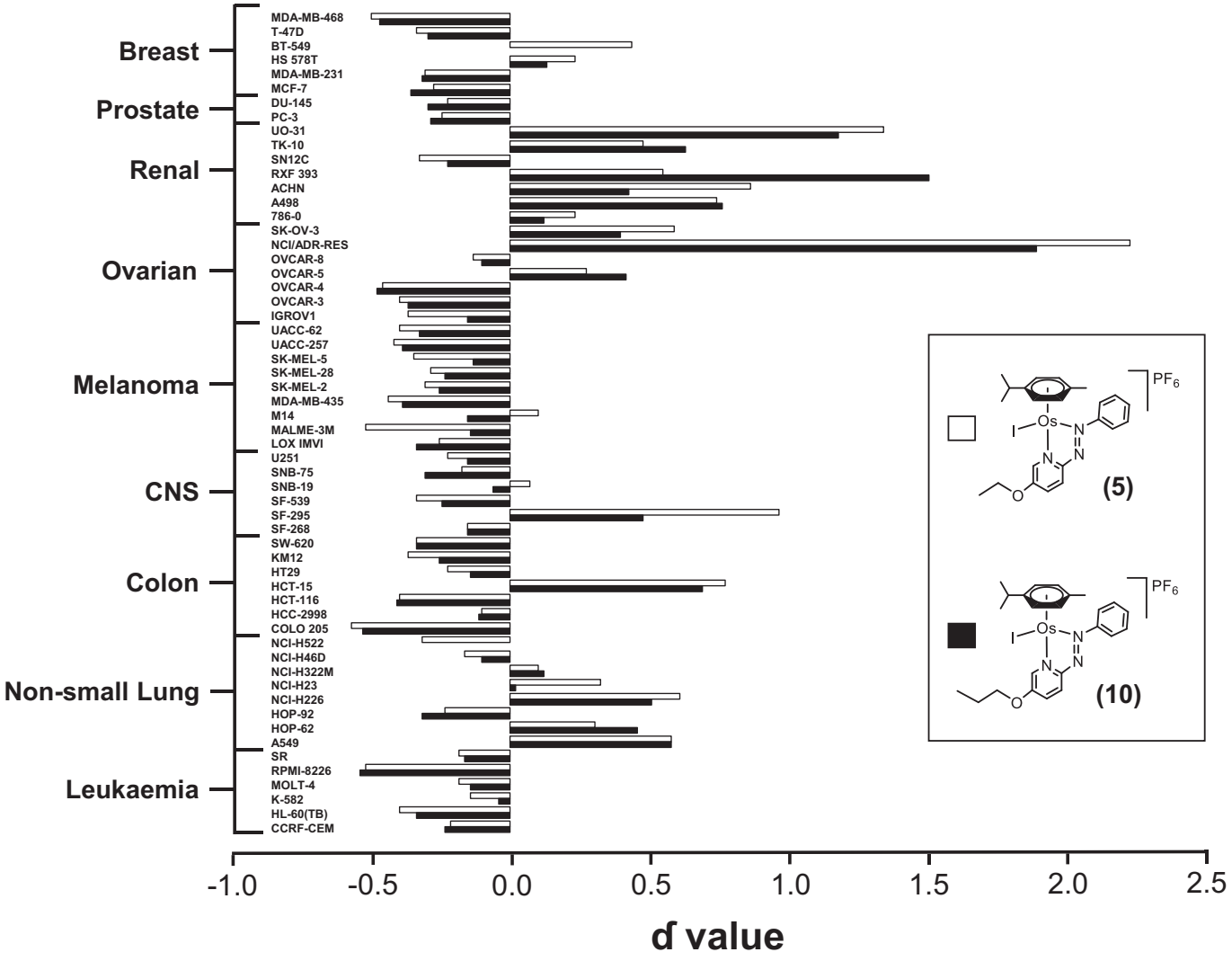

Fig. 9. Mean Log_{10} GI_{50} values for complexes **5** and **10** in the NCI 60-cell line panel. Bars to the right indicate activity lower than the mean. Mean for **5** and **10** is 0.42 μM.

Table 4
The six most significant correlations between antiproliferative data on NCI-60 cell lines for complexes **5** and **10** and compounds in the NCI 'synthetics' database generated using the COMPARE algorithm.

	Pearson correlation coefficient					
Complex	**Olivomycin**	**Gamitrinib-TTP**	**Phemerol**	**Phyllanthoside**	**Rubremetinium chloride**	**Bouvardin**
5	0.865	0.855	0.886	0.826	0.818	0.816
10	0.849	0.840	0.854	0.847	0.833	0.867

Abbreviations

AZPY	Azopyridine
Bip	Biphenyl
CHN	Carbon, hydrogen and nitrogen elemental analysis
ESI-MS	Electrospray ionisation mass spectrometry
GI_{50}	Concentration for 50% inhibition of cell growth (NCI)
IC_{50}	Concentration for 50% of maximum inhibition of cell growth
ICP-MS	Inductively coupled plasma-mass spectometry
ICP-OES	Inductively coupled plasma-optical emission spectroscopy
K	Capacity factor
NCI	National Cancer Institute
OSW	Octanol-saturated water
PBS	Phosphate buffered saline solution
p-cym	*para*-cymene
$P_{o/w}$	Octanol-water partition coefficient
Ro5	Lipinski's 'rule of five'
ROS	Reactive oxygen species
RP-HPLC	Reverse-phase high-pressure liquid chromatography
SARs	Structure-activity relationships
SF	Selectivity factor
WSO	Water-saturated octanol

Acknowledgements

We thank the ERC (grant nos. 247450, 324594), EPSRC (grant nos.

EP/F034210/1 and EP/P030572/1), Mike and Enfys Bagguley, (PhD Studentship for HEB), the Wellcome Trust (grant no. 107691/Z/15/Z), and Anglo American Platinum, for their support for this project. We also thank Heraeus for the gift of some osmium, the National Cancer Institute for NCI-60 screening, Wen-Ying Zhang, Dr. Lijiang Song and Dr. Ivan Prokes for assistance with electrochemistry, ICP-OES, ICP-MS, ESI-MS, and NMR, and Dr. Jessica M. Hearn for helpful discussion of NCI data.

Declaration of competing interest

The authors have no conflicts of interest.

Appendix A. Supplementary data

Experimental data on the synthesis and characterisation of complexes and ligands, experimental techniques, methods and assays, crystallographic data, reaction schemes, water stability and additional electrochemical data, correlation plots, biological assay data, NCI-60 one dose response data, and a detailed explanation of solubility, lipophilicity and anticancer activity trends. Supplementary data to this article can be found online at doi: https://doi.org/10.1016/j.jinorgbio.2020.111154.

References

[1] R.A. Krause, K. Krause, Inorg. Chem. 19 (1980) 2600–2603.
[2] S.J. Dougan, A. Habtemariam, S.E. McHale, S. Parsons, P.J. Sadler, Proc. Natl. Acad. Sci. U. S. A. 105 (2008) 11628–11633.
[3] S.J. Dougan, M. Melchart, A. Habtemariam, S. Parsons, P.J. Sadler, Inorg. Chem. 45 (2006) 10882–10894.
[4] Y. Fu, A. Habtemariam, A.M.B.H. Basri, D. Braddick, G.J. Clarkson, P.J. Sadler, Dalton Trans. 40 (2011) 10553–10562.
[5] Y. Fu, A. Habtemariam, A.M. Pizarro, S.H. van Rijt, D.J. Healey, P.A. Cooper, S.D. Shnyder, G.J. Clarkson, P.J. Sadler, J. Med. Chem. 53 (2010) 8192–8196.
[6] S.S.H. van Rijt, I. Romero-Canelón, Y. Fu, S.D. Shnyder, P.J. Sadler, Metallomics 6 (2014) 1014–1022.
[7] F. Baumann, W. Kaim, G. Denninger, H.J. Kümmerer, J. Fiedler, Organometallics 24 (2005) 1966–1973.
[8] J.M. Hearn, I. Romero-Canelón, A.F. Munro, Y. Fu, A.M. Pizarro, M.J. Garnett, U. McDermott, N.O. Carragher, P.J. Sadler, Proc. Natl. Acad. Sci. U. S. A. 112 (2015) E3800–E3805.
[9] A.M. Pizarro, A. Habtemariam, P.J. Sadler, Top. Organomet. Chem. 32 (2010) 21–56.
[10] A.F.A. Peacock, A. Habtemariam, R. Fernández, V. Walland, F.P.A. Fabbiani, S. Parsons, R.E. Aird, D.I. Jodrell, P.J. Sadler, J. Am. Chem. Soc. 128 (2006) 1739–1748.
[11] A.F.A. Peacock, A. Habtemariam, S.A. Moggach, A. Prescimone, S. Parsons, P.J. Sadler, Inorg. Chem. 46 (2007) 4049–4059.
[12] A.F.A. Peacock, S. Parsons, P.J. Sadler, J. Am. Chem. Soc. 129 (2007) 3348–3357.
[13] H. Kostrhunova, J. Florian, O. Novakova, A.F.A. Peacock, P.J. Sadler, V. Brabec, J. Med. Chem. 51 (2008) 3635–3643.
[14] I. Romero-Canelón, M. Mos, P.J. Sadler, J. Med. Chem. 58 (2015) 7874–7880.
[15] Y. Fu, M.J. Romero, A. Habtemariam, M.E. Snowden, L. Song, G.J. Clarkson, B. Qamar, A.M. Pizarro, P.R. Unwin, P.J. Sadler, Chem. Sci. 3 (2012) 2485–2494.
[16] C.A. Lipinski, F. Lombardo, B.W. Dominy, P.J. Feeney, Adv. Drug Deliver. Rev. 23 (1997) 3–25.
[17] C.A. Lipinski, Drug Discov. Today Technol. 1 (2004) 337–341.
[18] A.K. Ghose, V.N. Viswanadhan, J.J. Wendoloski, J. Comb. Chem. 1 (1999) 55–68.
[19] P.O. Asekunowo, R.A. Haque, M.R. Razali, Rev. Inorg. Chem. 37 (2017) 29–50.
[20] Y.R. Zheng, K. Suntharalingam, T.C. Johnstone, H. Yoo, W. Lin, J.G. Brooks, S.J. Lippard, J. Am. Chem. Soc. 136 (2014) 8790–8798.
[21] E.S. Barskaya, V.V. Shorokhov, A.V. Rzheutsky, A.D. Khudyakov, I.V. Yudin, V.A. Tafeenko, N.V. Zyk, E.K. Beloglazkina, Russ. Chem. Bull. 68 (2019) 638–643.
[22] N.M.R. McNeil, D.J. Press, D.M. Mayder, P. Garnica, L.M. Doyle, T.G. Back, J. Org. Chem. 81 (2016) 7884–7897.
[23] Y. Li, T. Zhang, Q. Liu, J. He, Front. Pharmacol. 10 (2019) 1–14.
[24] L.K. Batchelor, E. Păunescu, M. Soudani, R. Scopelliti, P.J. Dyson, Inorg. Chem. 56 (2017) 9617–9633.
[25] S. Stahl, H. Werner, Organometallics 9 (1990) 1876–1881.
[26] J. Tönnemann, J. Risse, Z. Grote, R. Scopelliti, K. Severin, Eur. J. Inorg. Chem. 2013 (2013) 4558–4562.
[27] H.S. Clayton, B.C.E. Makhubela, H. Su, G.S. Smith, J.R. Moss, Polyhedron 28 (2009) 1511–1517.
[28] G. Sheldrick, Acta Crystallogr. A 46 (1990) 467–473.
[29] M. Henczi, J. Nagy, D.F. Weaver, J. Liq. Chromatogr. 17 (1994) 2605–2613.
[30] K. Taka'cs-Nova'k, A. Avdeel, J. Pharm. Biomed. Anal. 14 (1996) 1405–1413.
[31] C. Venzago, M. Popp, J. Kovac, A. Kunkel, J. Anal. At. Spectrom. 28 (2013) 1125–1129.
[32] R.J. Needham, C. Sanchez-Cano, X. Zhang, I. Romero-Canelón, A. Habtemariam, M.S. Cooper, L. Meszaros, G.J. Clarkson, P.J. Blower, P.J. Sadler, Angew. Chem. Int. Ed. 56 (2017) 1017–1020.
[33] C. Martorell, A.C. Calpena, E. Escribano, J.M. Poblet, J. Freixas, J. Chromatogr. A 655 (1993) 177–184.
[34] M.H.M. Klose, S. Theiner, H.P. Varbanov, D. Hoefer, V. Pichler, M. Galanski, S.M. Meier-Menches, B.K. Keppler, Inorganics 6 (2018) 130.
[35] J. Saab, G. Bassil, R. Abou Naccoul, J. Stephan, I. Mokbel, J. Jose, Chemosphere 82 (2011) 929–934.
[36] C. Yokoyama, M. Terui, S. Takahashi, Fluid Phase Equilib. 82 (1993) 283–290.
[37] A. Noubigh, M. Abderrabba, E. Provost, J. Iran. Chem. Soc. 6 (2009) 168–176.
[38] S.K. Sahu, G.G. Pandit, J. Liq. Chromatogr. R. T. 26 (2003) 135–146.
[39] S. Samanta, P. Ghosh, S. Goswami, Dalton Trans. 41 (2012) 2213–2226.
[40] I. Romero-Canelón, L. Salassa, P.J. Sadler, J. Med. Chem. 56 (2013) 1291–1300.
[41] M. López-Lázaro, Cancer Lett. 252 (2007) 1–8.
[42] M.P. Lisanti, U.E. Martinez-Outschoorn, Z. Lin, S. Pavlides, D. Whitaker-Menezes, R.G. Pestell, A. Howell, F. Sotgia, Cell Cycle 10 (2011) 2440–2449.
[43] T.P. Szatrowski, C.F. Nathan, Cancer Res. 51 (1991) 794–798.
[44] U. Jungwirth, C.R. Kowol, B.K. Keppler, C.G. Hartinger, W. Berger, P. Heffeter, Antioxid. Redox Sign. 15 (2011) 1085–1127.
[45] J. Zhou, A.I. Marcus, S.L. Holbeck, P. Giannakakou, Cancer Res. 65 (2005) 7.
[46] D.W. Zaharevitz, S.L. Holbeck, C. Bowerman, P.A. Svetlik, J. Mol. Graph. Model. 20 (2002) 297–303.
[47] D.C. Ward, E. Reich, I.H. Goldberg, Science 149 (1965) 1259–1263.
[48] N. Garreau de Loubresse, I. Prokhorova, W. Holtkamp, M. Rodnina, G. Yusupova, M. Yusupov, Nature 513 (2014) 517–522.
[49] J.M. Hearn, G.M. Hughes, I. Romero-Canelón, A.F. Munro, B. Rubio-Ruiz, Z. Liu, N.O. Carragher, P.J. Sadler, Metallomics 10 (2018) 93–107.
[50] D.L. Boger, M.A. Patane, J. Zhou, J. Am. Chem. Soc. 116 (1994) 8544–8556.
[51] H. Kim, J. Yang, M.J. Kim, S. Choi, J.R. Chung, J.M. Kim, Y.H. Yoo, J. Chung, H. Koh, J. Biol. Chem. 291 (2015) 1841–1853.
[52] Y. Kaziro, M. Kamiyama, Biochem. Biophys. Res. Comm. 19 (1965) 433–437.
[53] G. Gasser, I. Ott, N. Metzler-Nolte, J. Med. Chem. 54 (2011) 3–25.
[54] S. Parveen, F. Arjmand, S. Tabassum, Eur. J. Med. Chem. 175 (2019) 269–286.
[55] I. Romero-Canelón, P.J. Sadler, Inorg. Chem. 52 (2013) 12276–12291.
[56] S.M. Meier-Menches, C. Gerner, W. Berger, C.G. Hartinger, B.K. Keppler, Chem. Soc. Rev. 47 (2018) 909–928.
[57] P. Zhang, H. Huang, Dalton Trans. 47 (2018) 14841–14854.
[58] M. Hanif, M.V. Babak, C.G. Hartinger, Drug Discov. Today 19 (2014) 1640–1648.
[59] P. Zhang, P.J. Sadler, J. Organomet. Chem. 839 (2017) 5–14.
[60] B. Cebrián-Losantos, A.A. Krokhin, I.N. Stepanenko, R. Eichinger, M.A. Jakupec, V.B. Arion, B.K. Keppler, Inorg. Chem. 46 (2007) 5023–5033.
[61] G.E. Büchel, I.N. Stepanenko, M. Hejl, M.A. Jakupec, B.K. Keppler, V.B. Arion, Inorg. Chem. 50 (2011) 7690–7697.
[62] W. Ginzinger, G. Mühlgassner, V.B. Arion, M.A. Jakupec, A. Roller, M. Galanski, M. Reithofer, W. Berger, B.K. Keppler, J. Med. Chem. 55 (2012) 3398–3413.
[63] K.J. Kilpin, S. Crot, T. Riedel, J.A. Kitchen, P.J. Dyson, Dalton Trans. 43 (2014) 1443–1448.
[64] H.K. Liu, J.A. Parkinson, J. Bella, F. Wang, P.J. Sadler, Chem. Sci. 1 (2010) 258–270.
[65] M. Ishikawa, Y. Hashimoto, J. Med. Chem. 54 (2011) 1539–1554.